Supplementary material for "Leveraging reforecasts for flood estimation with long continuous simulation: a proof-of-concept study"

Daniel Viviroli[1], **Martin Jury**[2], **Maria Staudinger**[1], **Martina Kauzlaric**[3,4], **Heimo Truhez**[2], **and Douglas Maraun**[2]

[1]Department of Geography, University of Zurich, Zurich, Switzerland
[2]Wegener Center for Climate and Global Change, University of Graz, Graz, Austria
[3]Institute of Geography, University of Bern, Bern, Switzerland
[4]Oeschger Centre for Climate Change Research, University of Bern, Bern,Switzerland

Correspondence: Daniel Viviroli (daniel.viviroli@geo.uzh.ch)

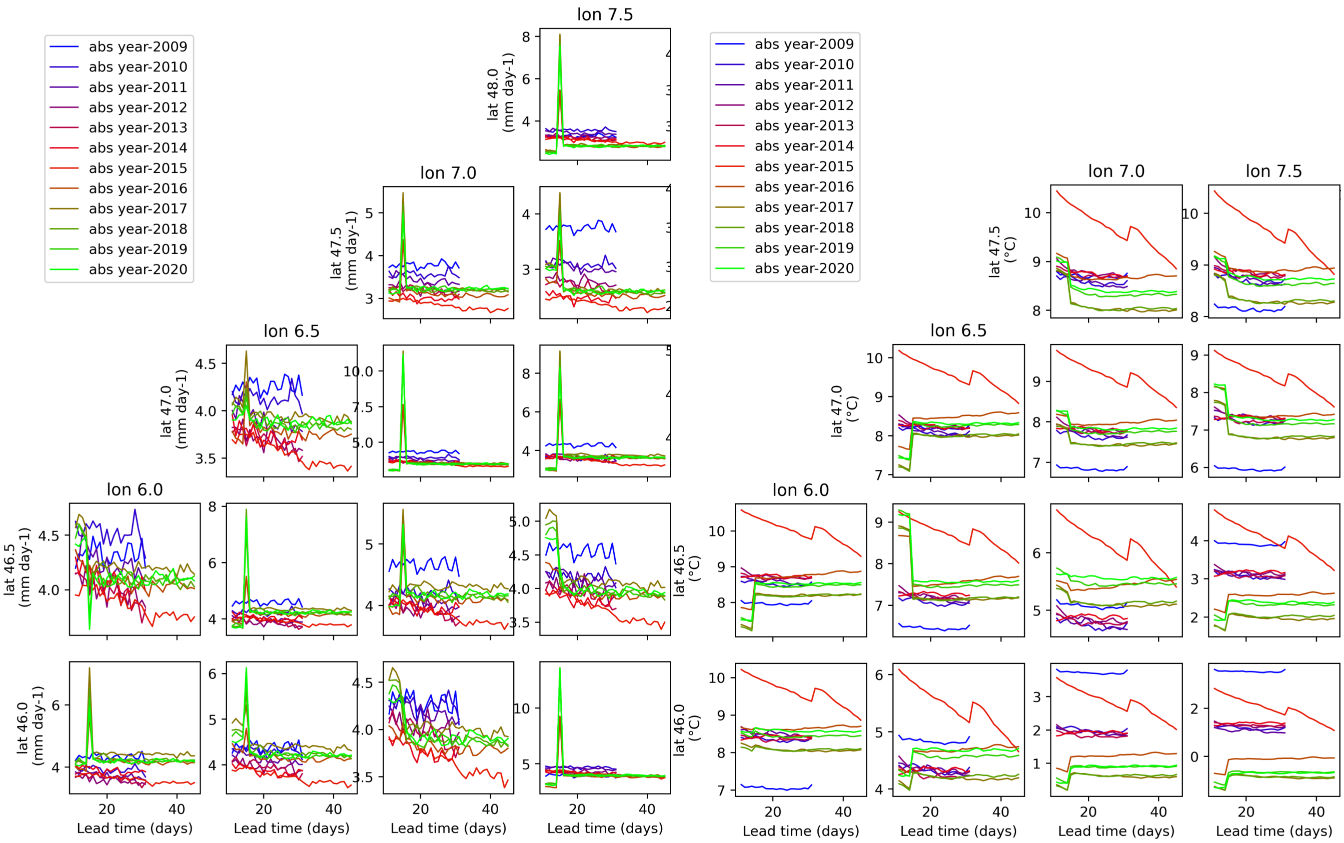

Figure S1. Annual mean ECMWF reforecast precipitation (left) and temperature (right) for selected grid points over Switzerland, plotted by forecast time (days 11 to 45) and by the year of initialization.

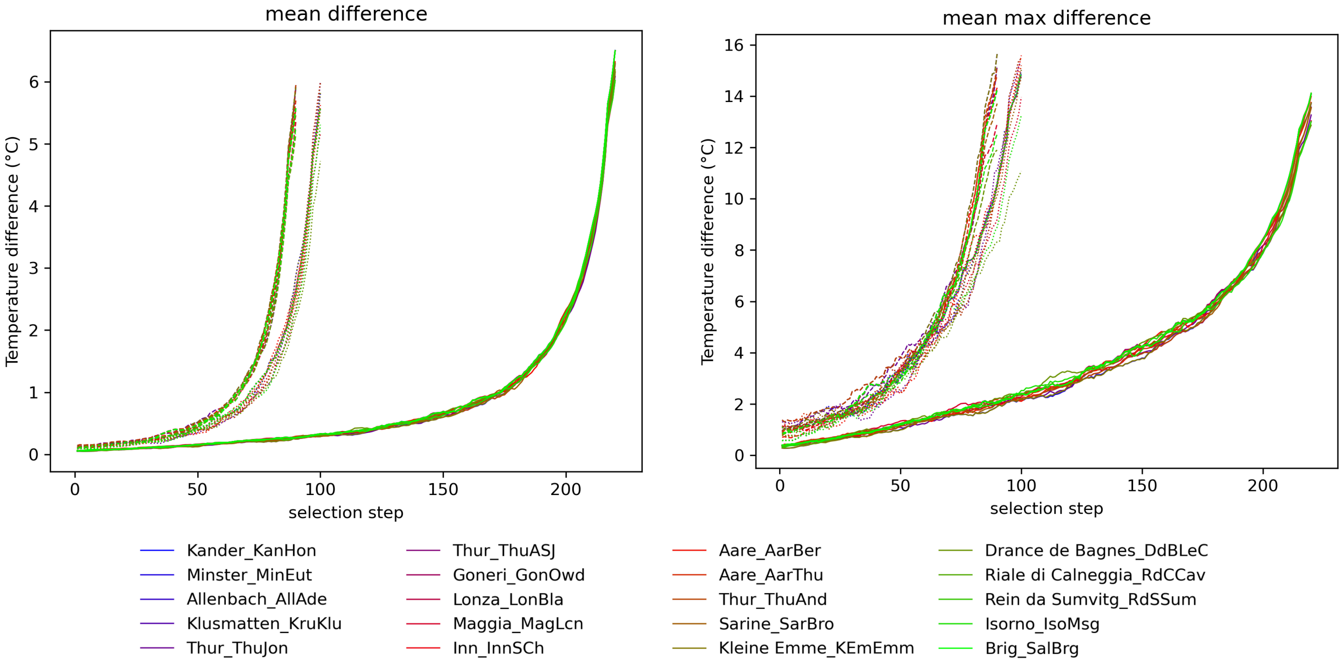

Figure S2. Mean (left) and maximum (right) 6-hourly raw temperature difference at the intersection time of concatenated single ECMWF RFs. Dashed lines are for RFs initialized between 2009–2012, dotted lines for RFs initialized between 2013–2014, and solid lines for RFs initialized between 2016–2020. A running mean of 11 selection steps was applied.

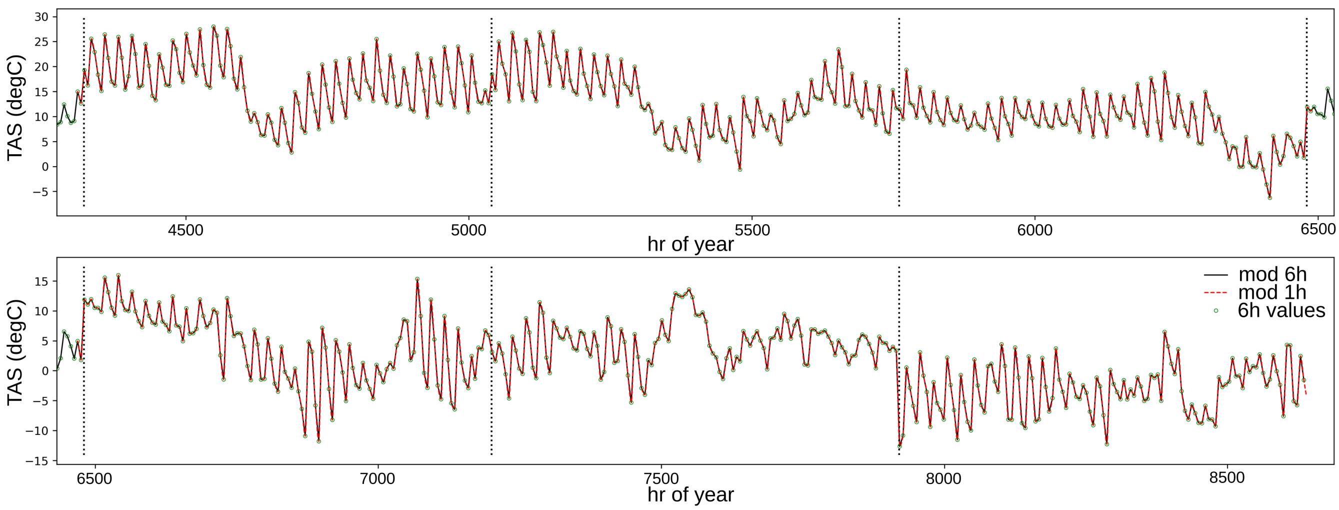

Figure S3. Time series of temperature (TAS) for the second half-year of one extreme 'gap'-year (year 9920) with an extreme temperature jump at the station Adelboden (ABO) in the Kander River catchment (at hr ~7900). The intercept between single reforecasts is indicated by the vertical dotted line.

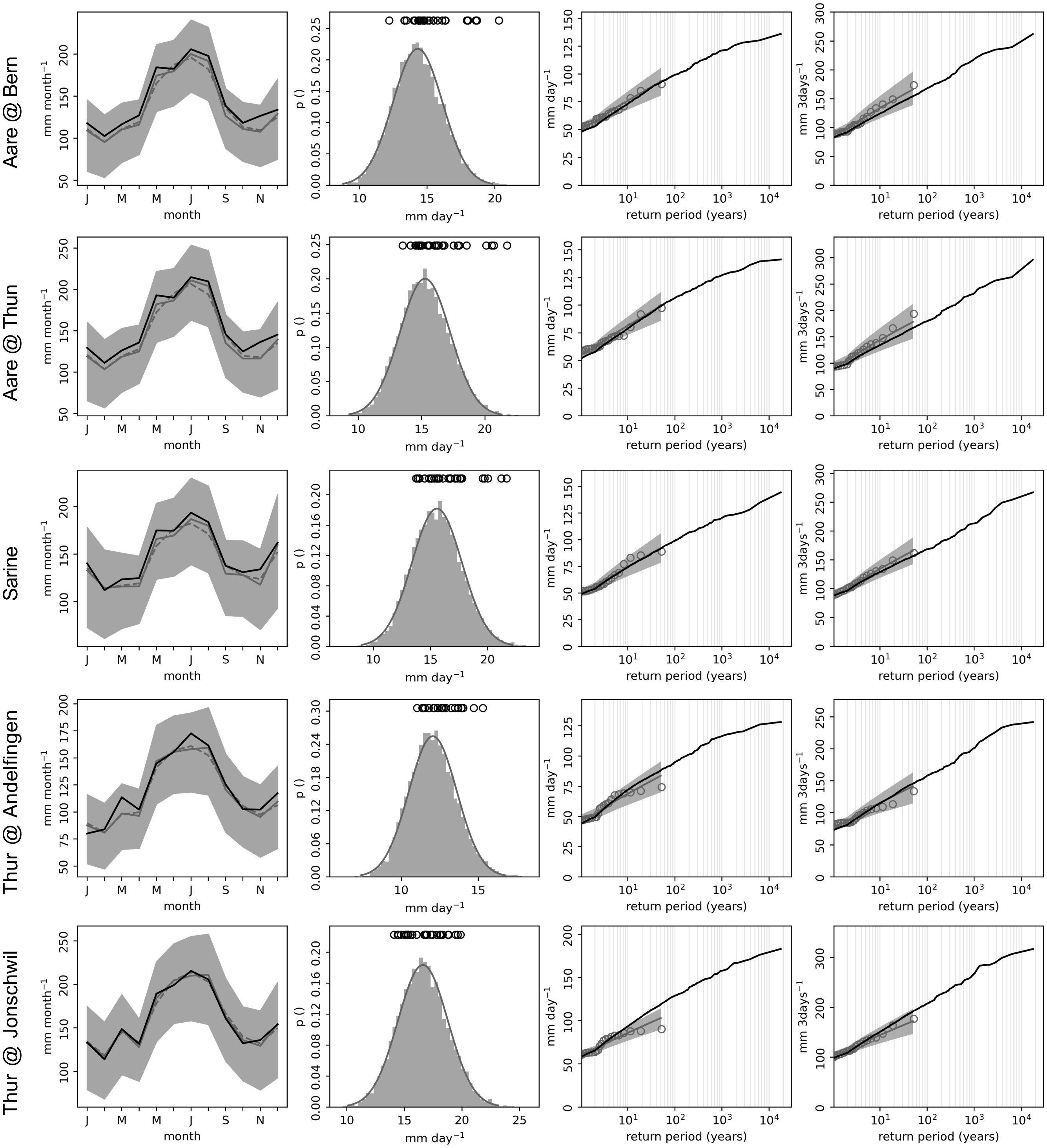

Figure S4. Evaluation of reforecast (RF) precipitation for large catchments: Aare at Bern, Aare at Thun, Sarine, Thur at Andelfingen, Thur at Jonschwil. From left to right: Annual cycle of mean monthly precipitation for observations (1991–2019, black) and RF (grey, shading p25–p75; dashed line based on 360-day calendar); histogram of annual daily p90 precipitation for RF, and observations (black circles); return levels for annual maximum daily and maximum 3-day precipitation for RF (black) and observation (grey circles) using the Gringorten plotting position. For observations, return values have additionally been fitted using a Gumbel distribution (using a GEV distribution resulted in overly broad confidence intervals) and maximum likelihood estimates, confidence intervals are based on 5000 bootstrap samples (mean in dark grey, p2.5–97.5 grey shading).

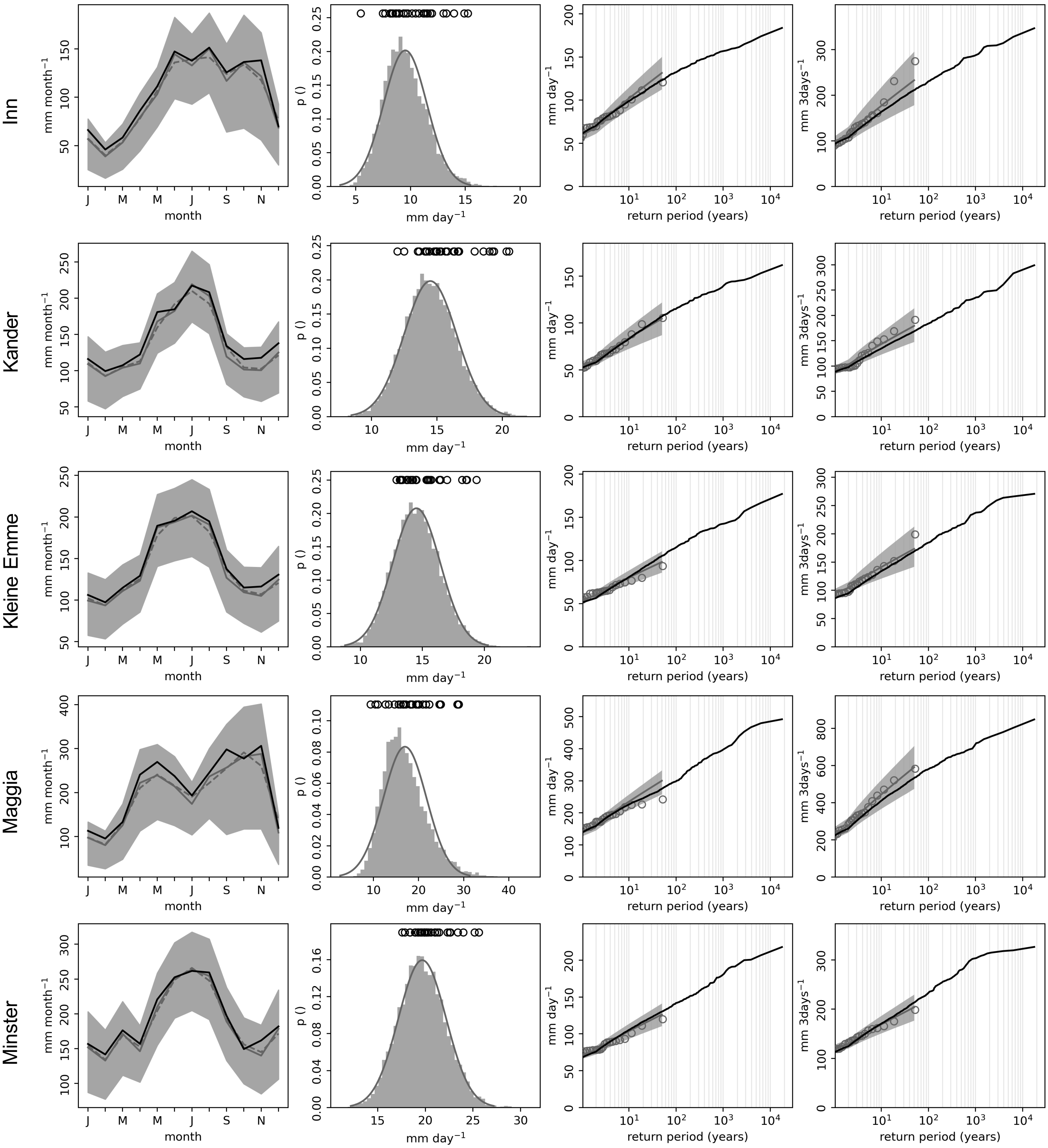

Figure S5. Same as Fig. S4, but for medium-sized catchments: Inn, Kander, Kleine Emme, Maggia, and Minster.

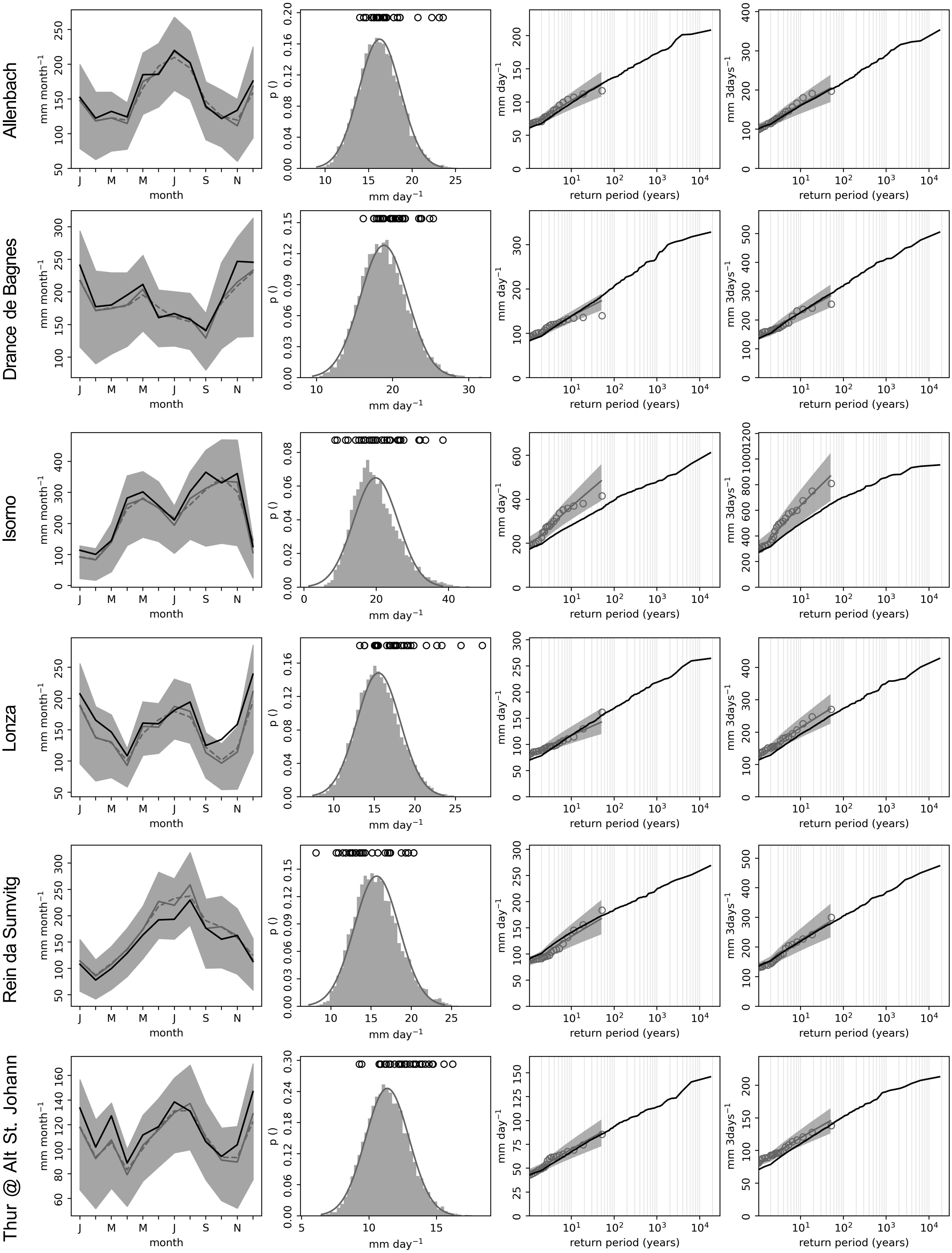

Figure S6. Same as Fig. S4, but for small catchments: Allenbach, Drance de Bagnes, Isorno, Lonza, Rein da Sumvitg and Thur at Alt St. Johann.

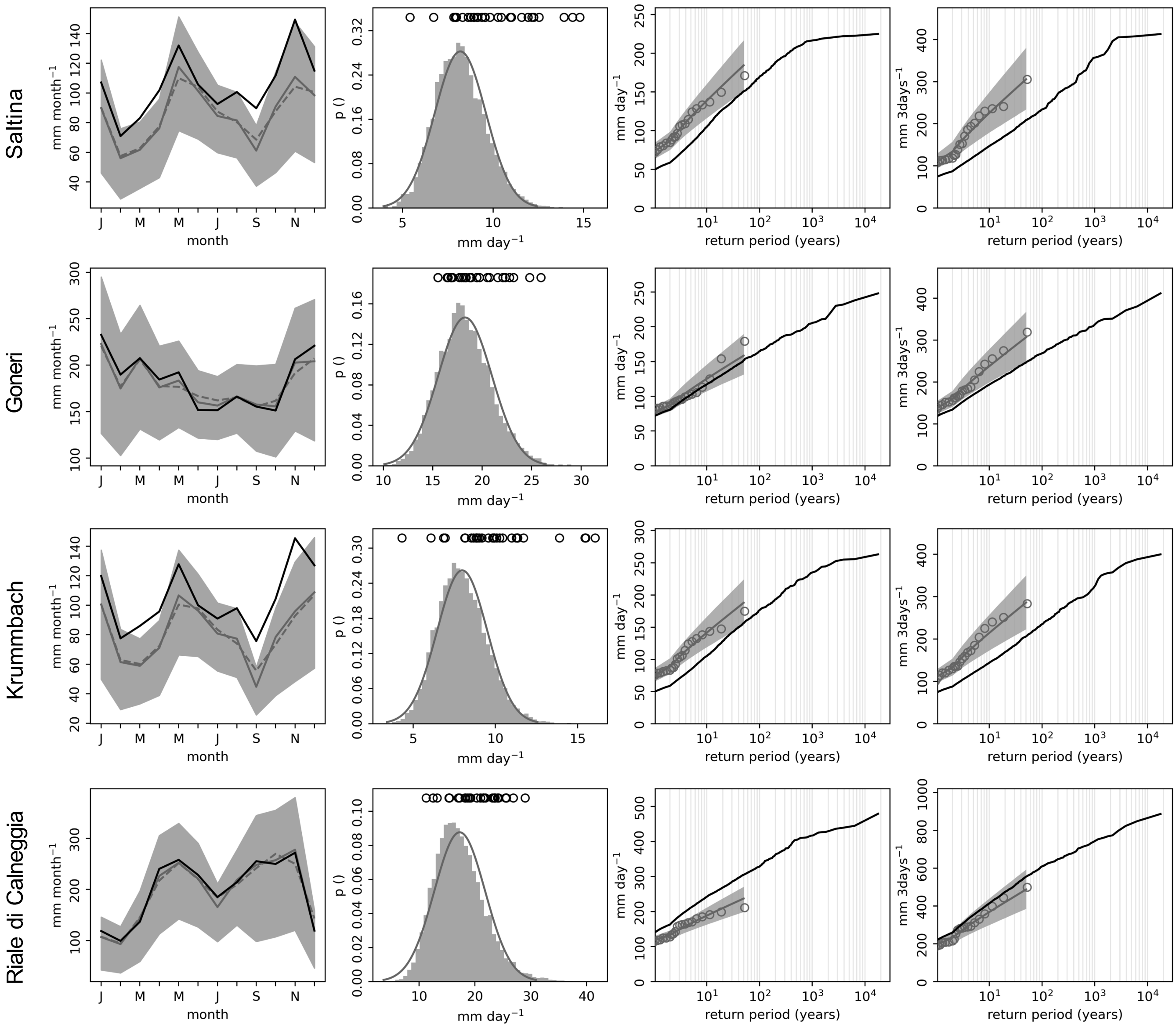

Figure S7. Same as Fig. S4, but for very small catchments: Saltina, Goneri, Krummbach and Riale di Calneggia.

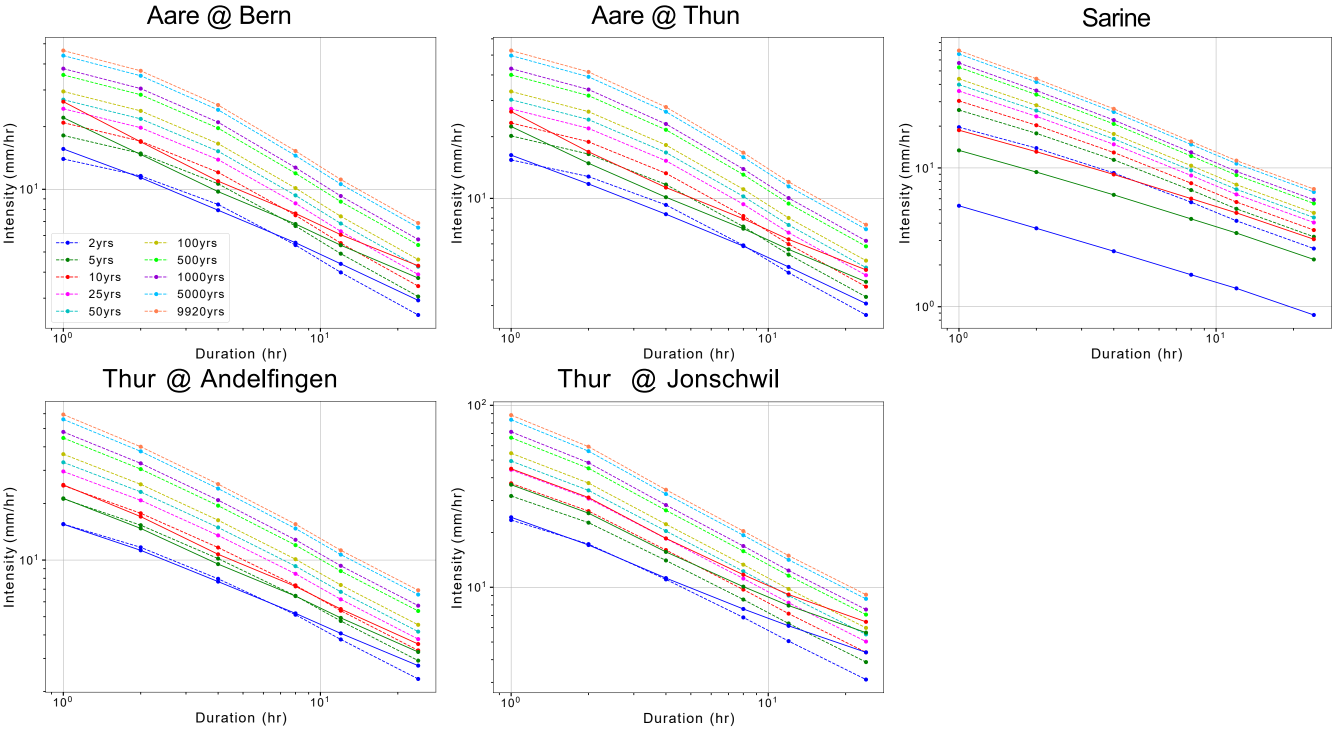

Figure S8. Average intensity-duration-frequency (IDF) curves (1h to 24h) for different return periods (colors) in large catchments: Aare at Bern, Aare at Thun, Sarine, Thur at Andelfingen and Thur at Jonschwil. Reforecasts results are shown with dashed lines, observations spanning 1981–2019 and used for the analog method are shown with solid lines. The IDFs have been derived using the Gumbel method (Ponce, 1989), and a 360-day calendar was used.

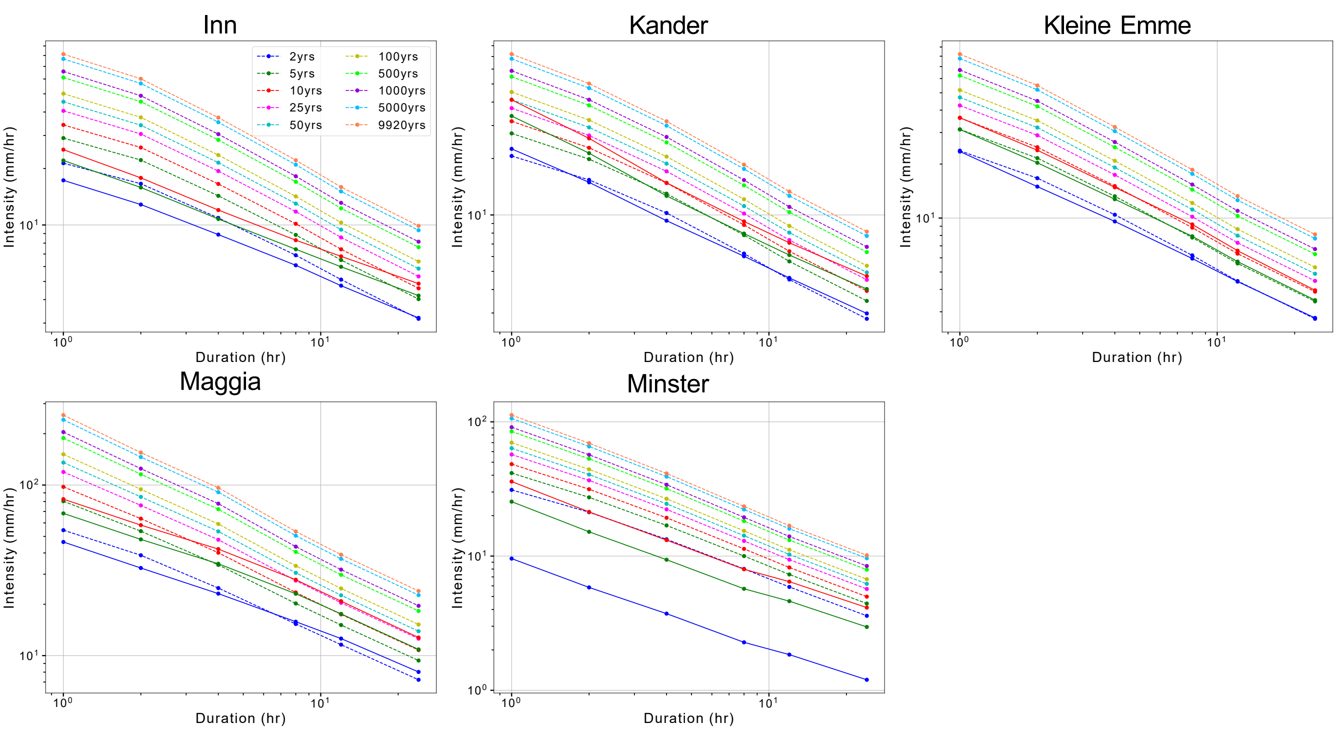

Figure S9. Same as Fig. S8 but for medium catchments: Inn, Kander, Kleine Emme, Maggia and Minster.

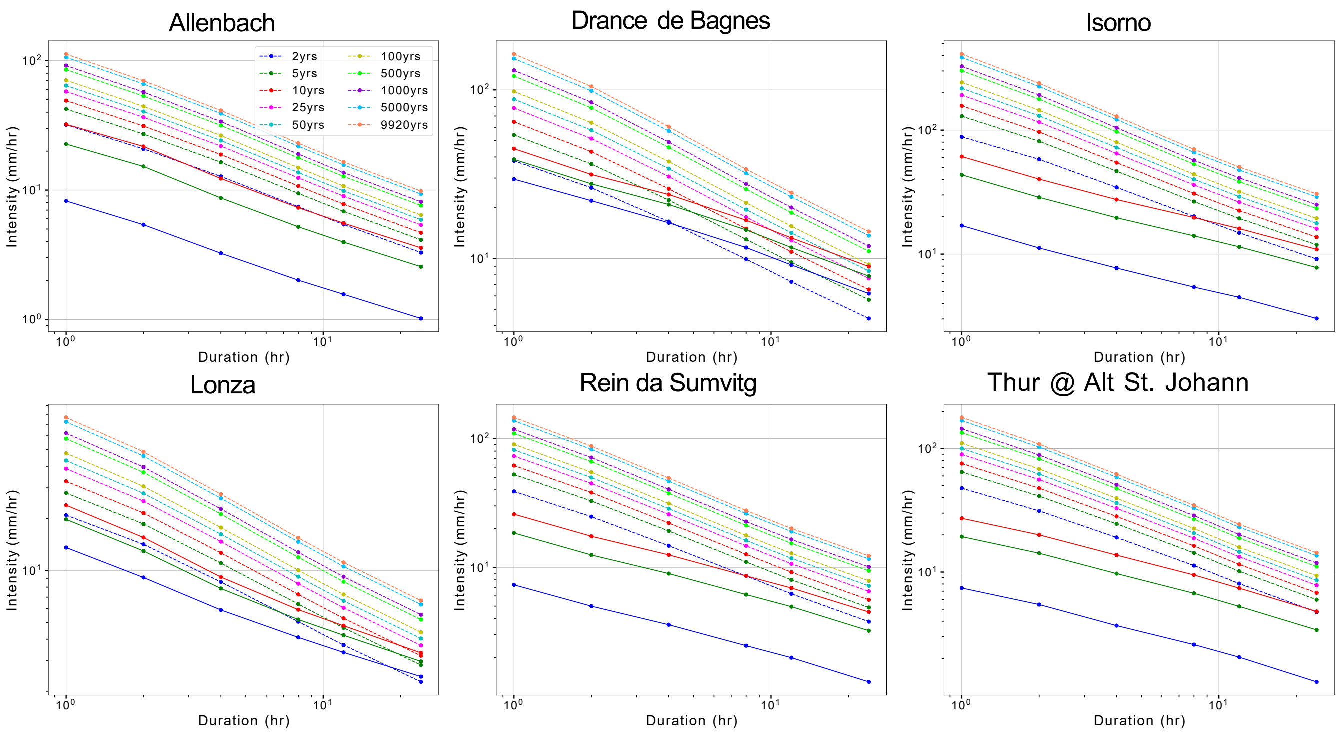

Figure S10. Same as Fig. S8 but for small catchments: Allenbach, Drance de Bagnes, Isorno, Lonza, Rein da Sumvitg and Thur at Alt St. Johann.

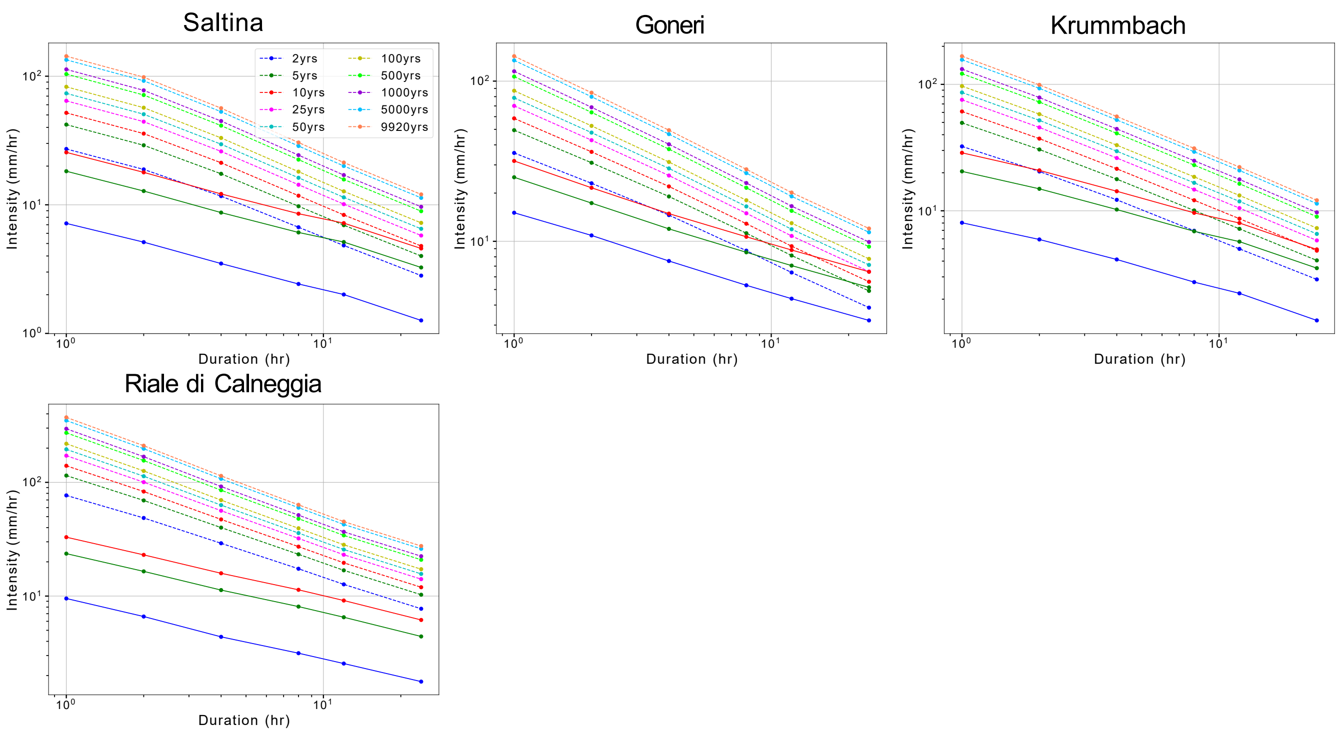

Figure S11. Same as Fig. S8 but for small catchments: Saltina, Goneri, Krummbach and Riale di Calneggia.

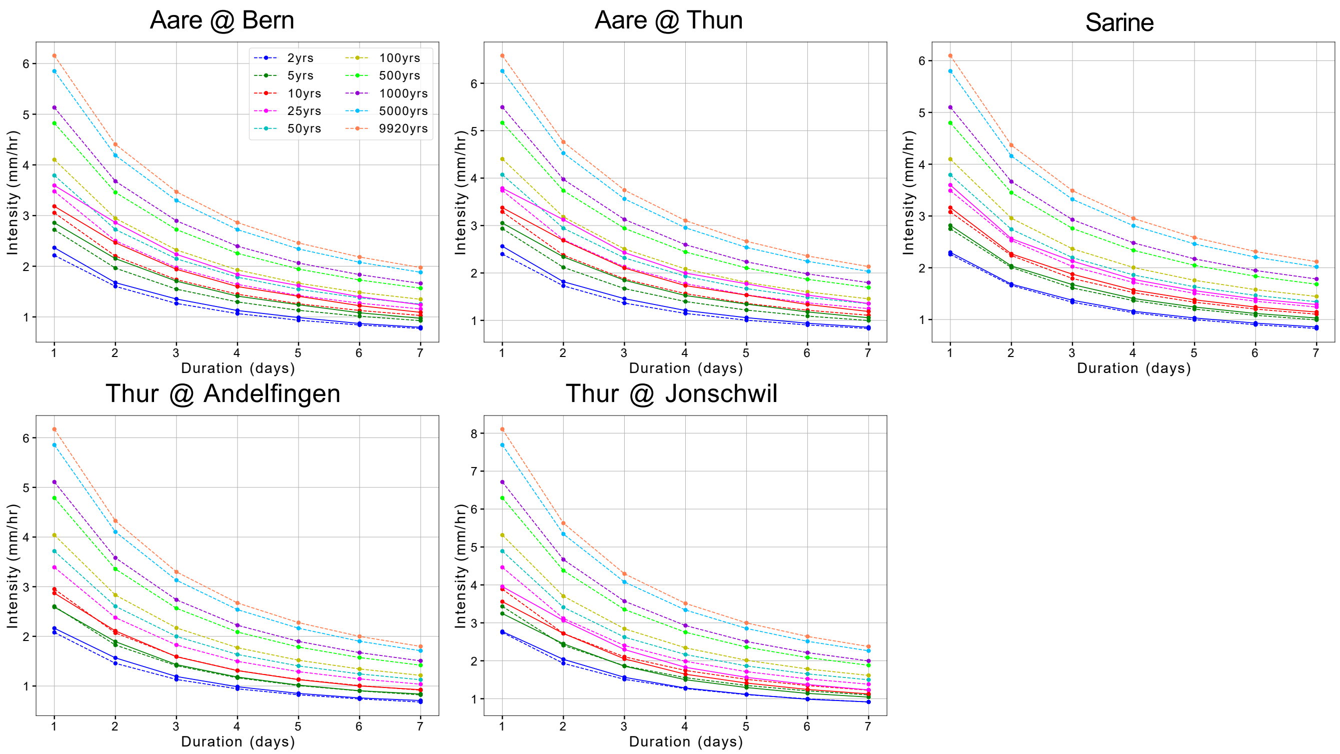

Figure S12. Average intensity-duration-frequency (IDF) curves (1-day to 7-days) for different return periods (colors) in large catchments: Aare at Bern, Aare at Thun, Sarine, Thur at Andelfingen and Thur at Jonschwil. Reforecasts results are shown with dashed lines, observations spanning 1981–2019 and used for the bias adjustment are shown with solid lines. The IDFs have been derived using the Gumbel method (Ponce, 1989), and a 360-day calendar was used.

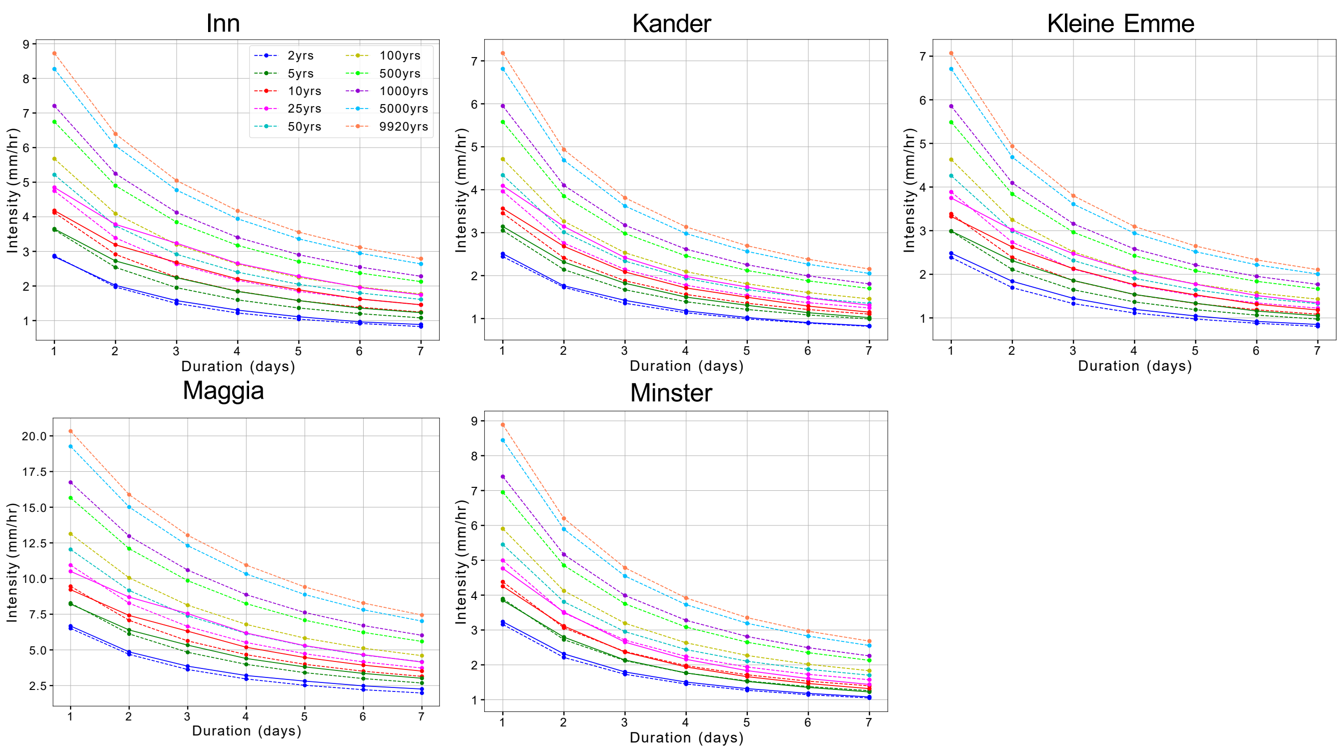

Figure S13. Same as Fig. S12 but for medium catchments: Inn, Kander, Kleine Emme, Maggia and Minster.

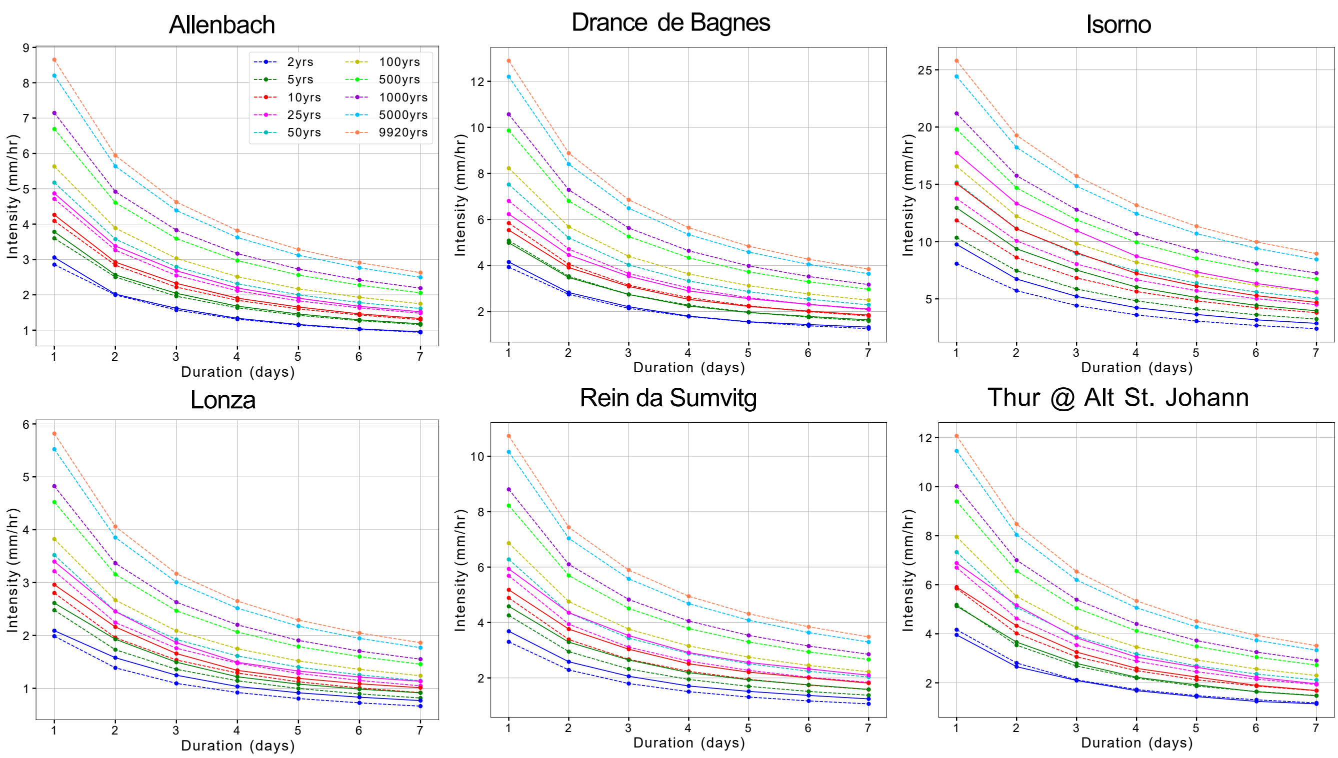

Figure S14. Same as Fig. S12 but for small catchments: Allenbach, Drance de Bagnes, Isorno, Lonza, Rein da Sumvitg and Thur at Alt St. Johann.

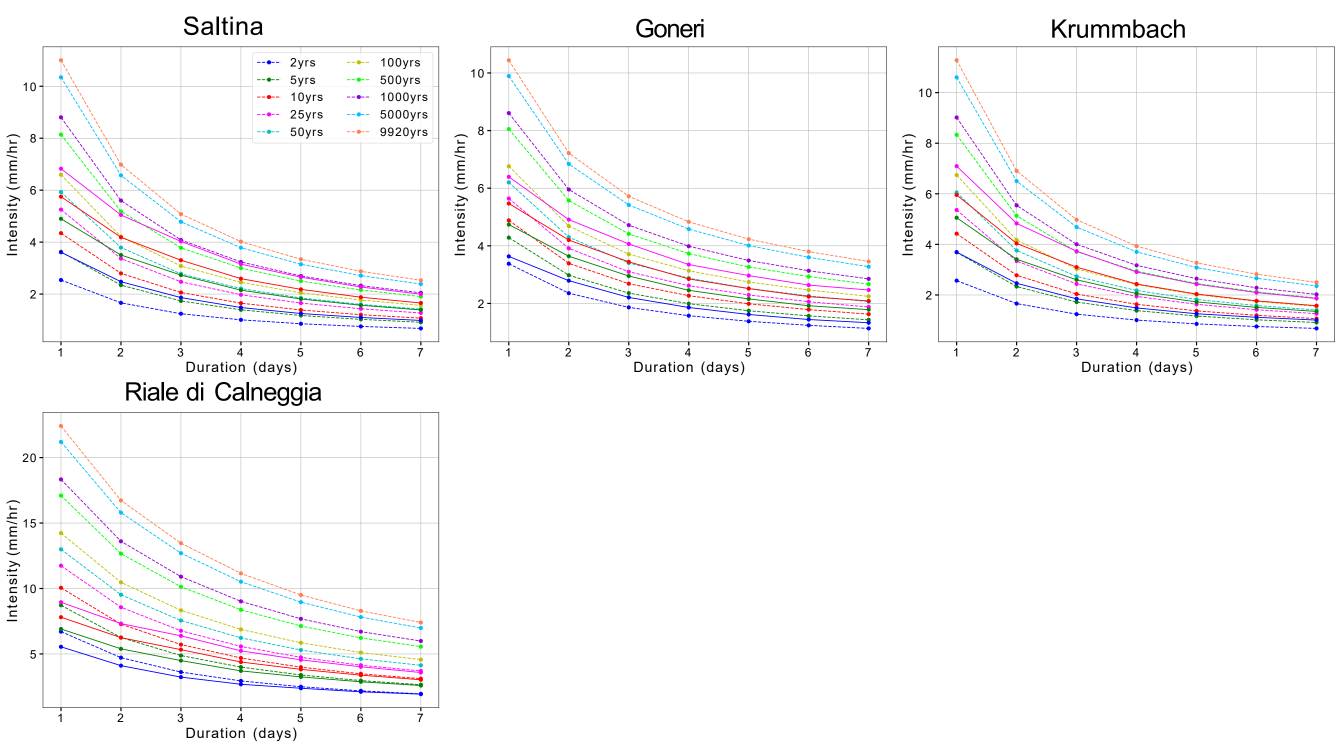

Figure S15. Same as Fig. S12 but for small catchments: Saltina, Goneri, Krummbach and Riale di Calneggia.

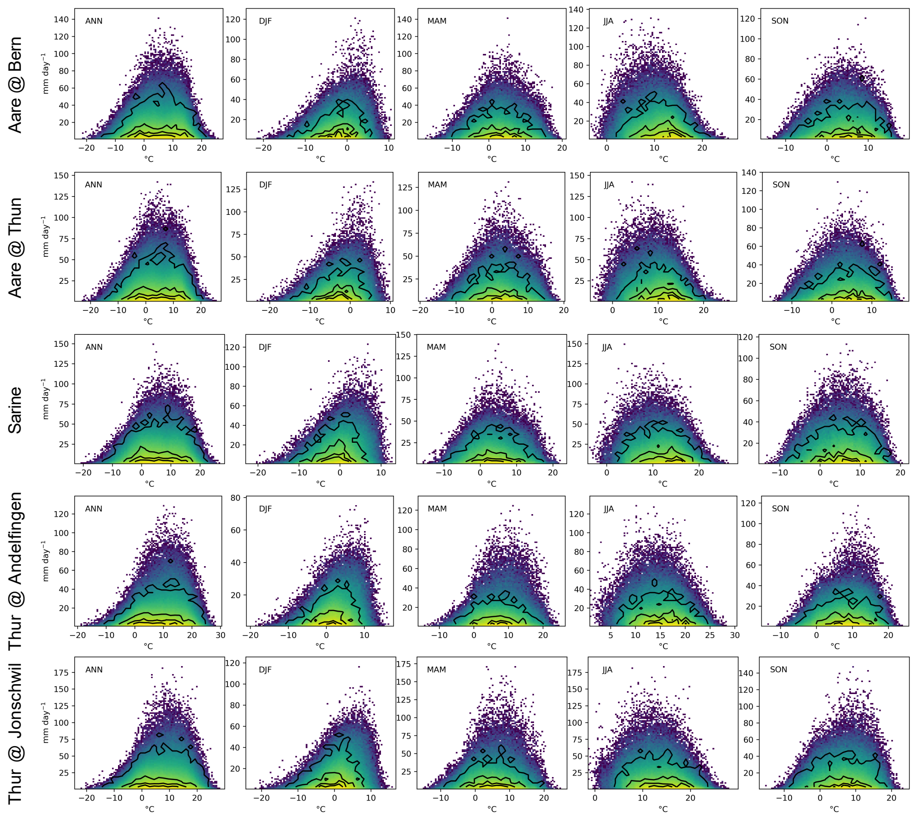

Figure S16. Annual and seasonal density plots based on daily mean temperature and precipitation (≥1 mm day^{-1}) and the final 360 day calendar for large catchments. Colours range from blue for low density to yellow high density. Observations over the 1991–2019 period are denoted by contour lines.

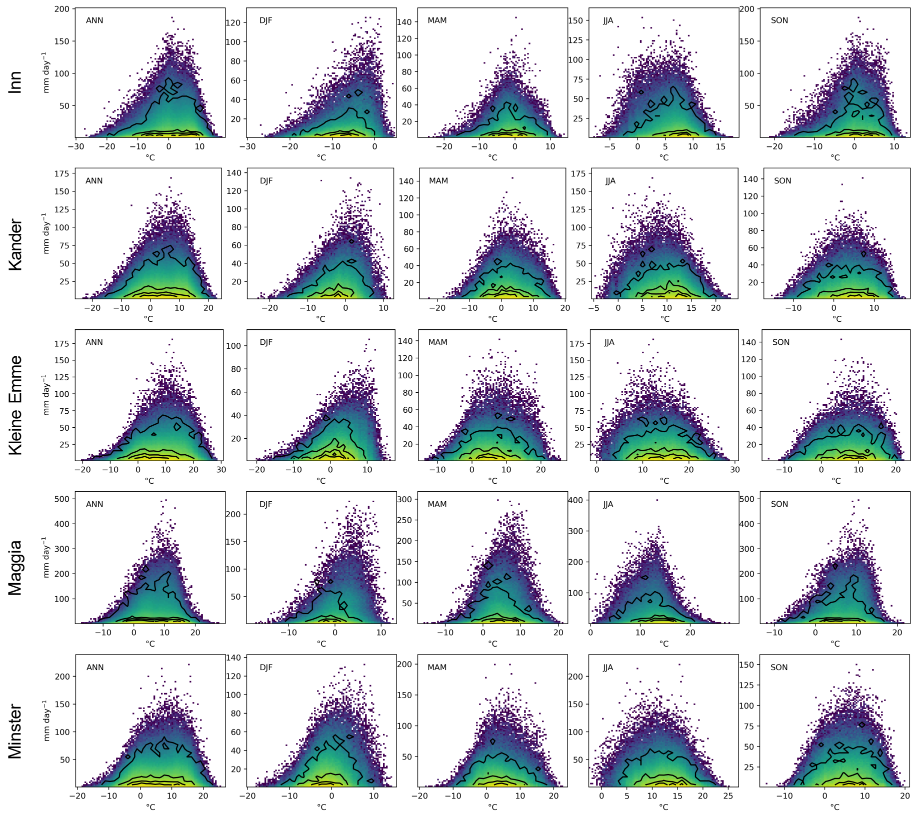

Figure S17. Same as Fig. S16, but for medium-sized catchments.

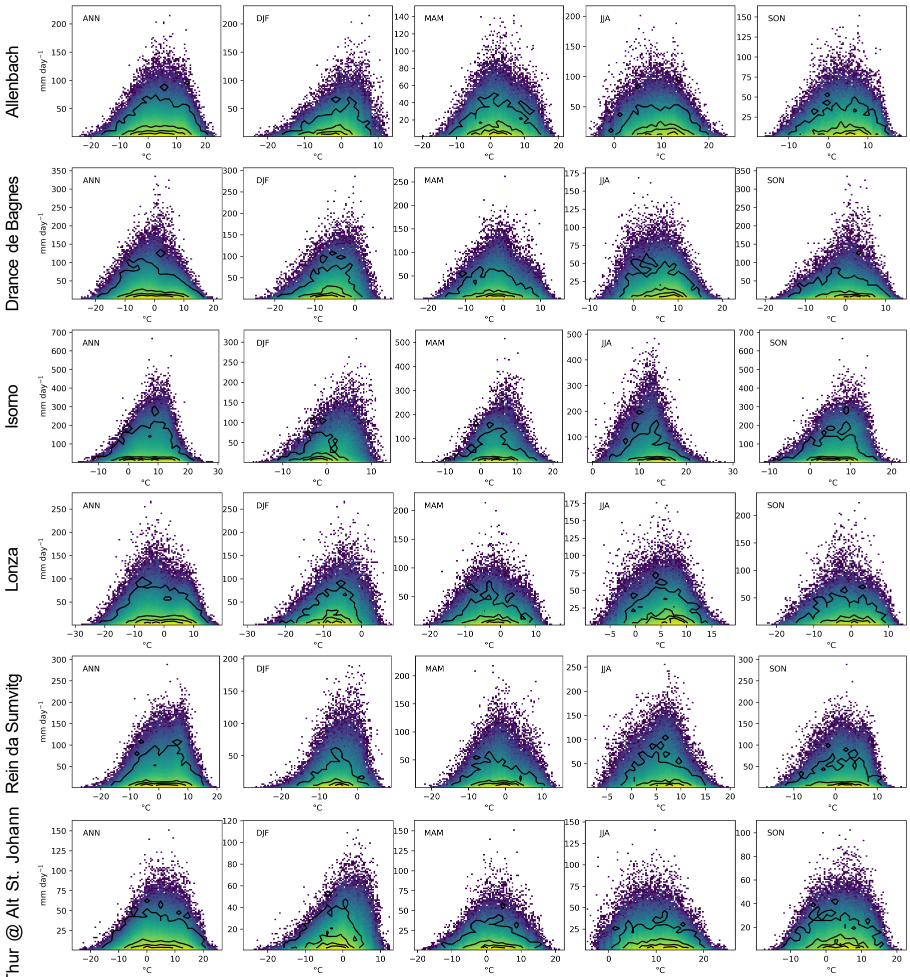

Figure S18. Same as Fig. S16, but for small catchments.

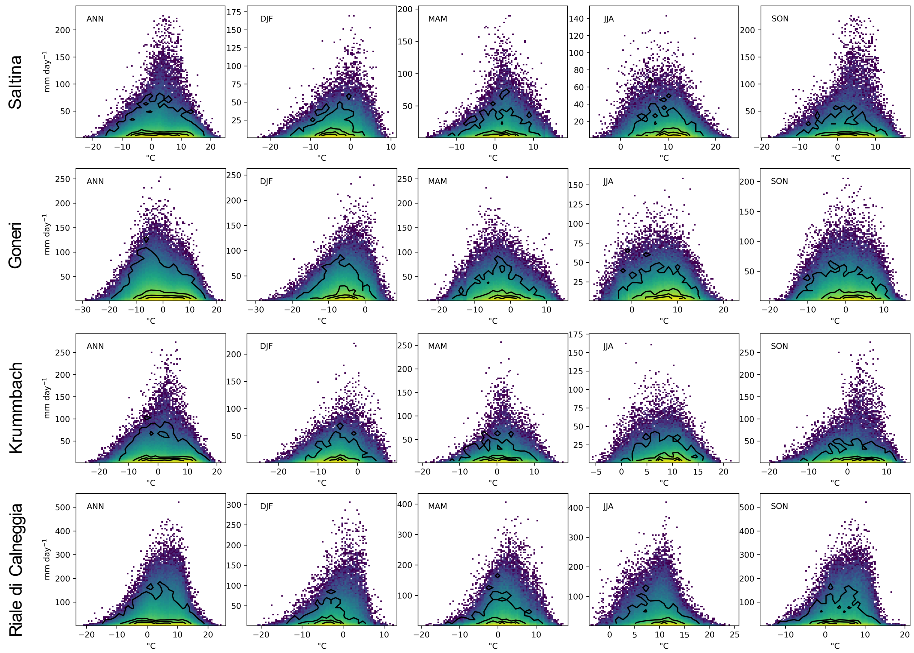

Figure S19. Same as Fig. S16, but for very small catchments.

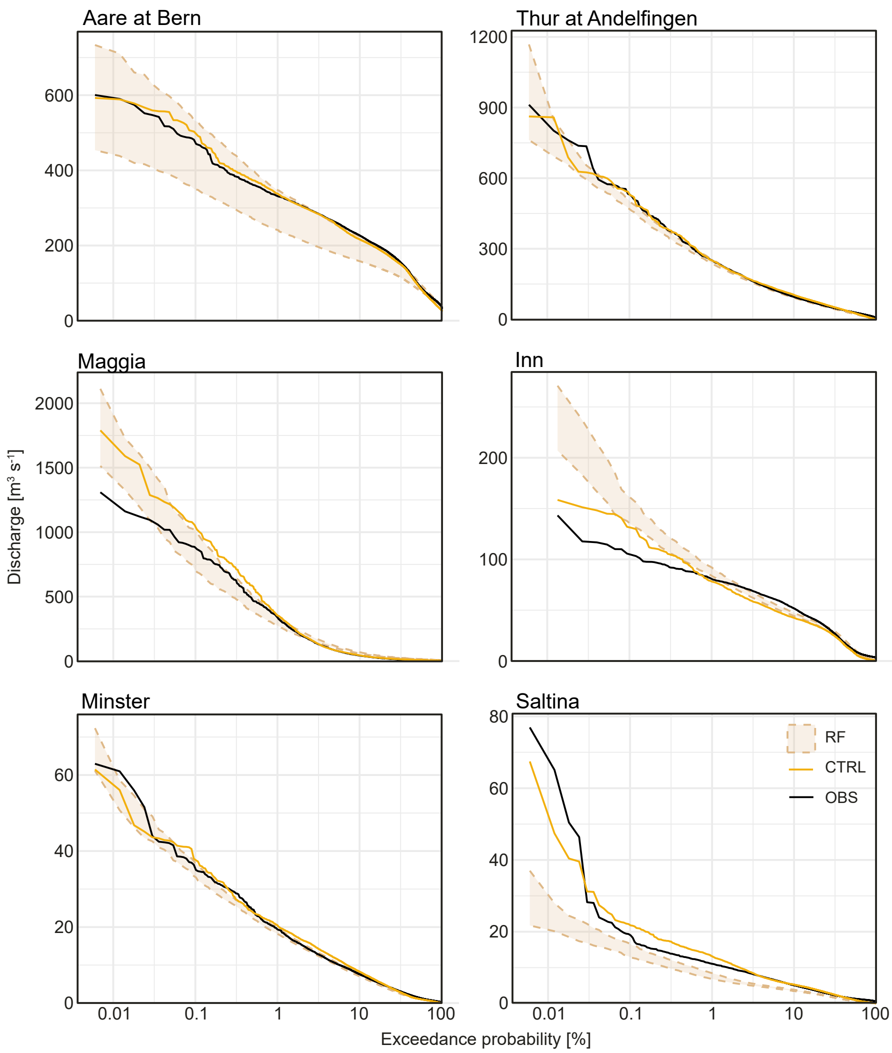

Figure S20. Flow Duration Curves (FDCs) for selected sites, comparing RF-based simulations (RF), control simulation (CTRL) and observations (OBS). Note that the x axis is scaled logarithmically. For RF-based simulations, samples matching the length of the observations (or, if shorter, the length of the control simulation) were taken, exceedance probabilities calculated, and 95% confidence intervals were computed.

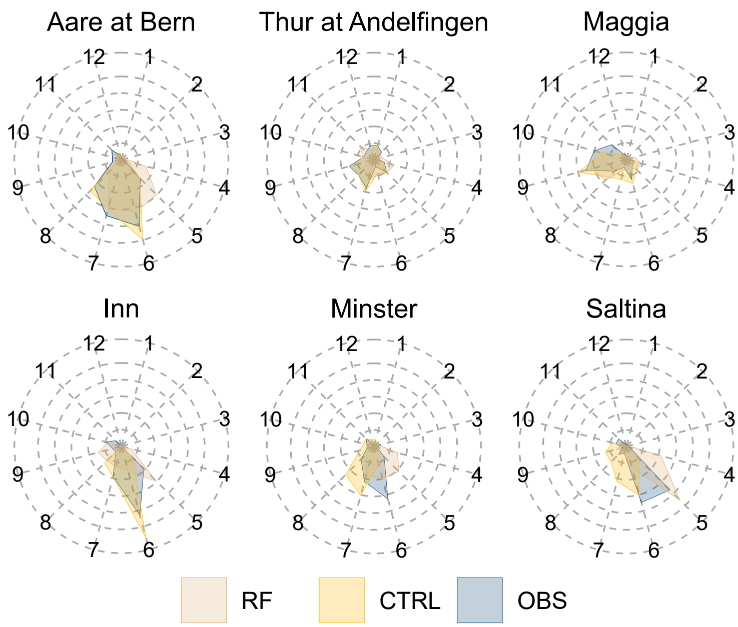

Figure S21. Seasonality of Annual Maximum Floods for selected sites, comparing reforecast-based simulations (RF), control simulation (CTRL) and observations (OBS).

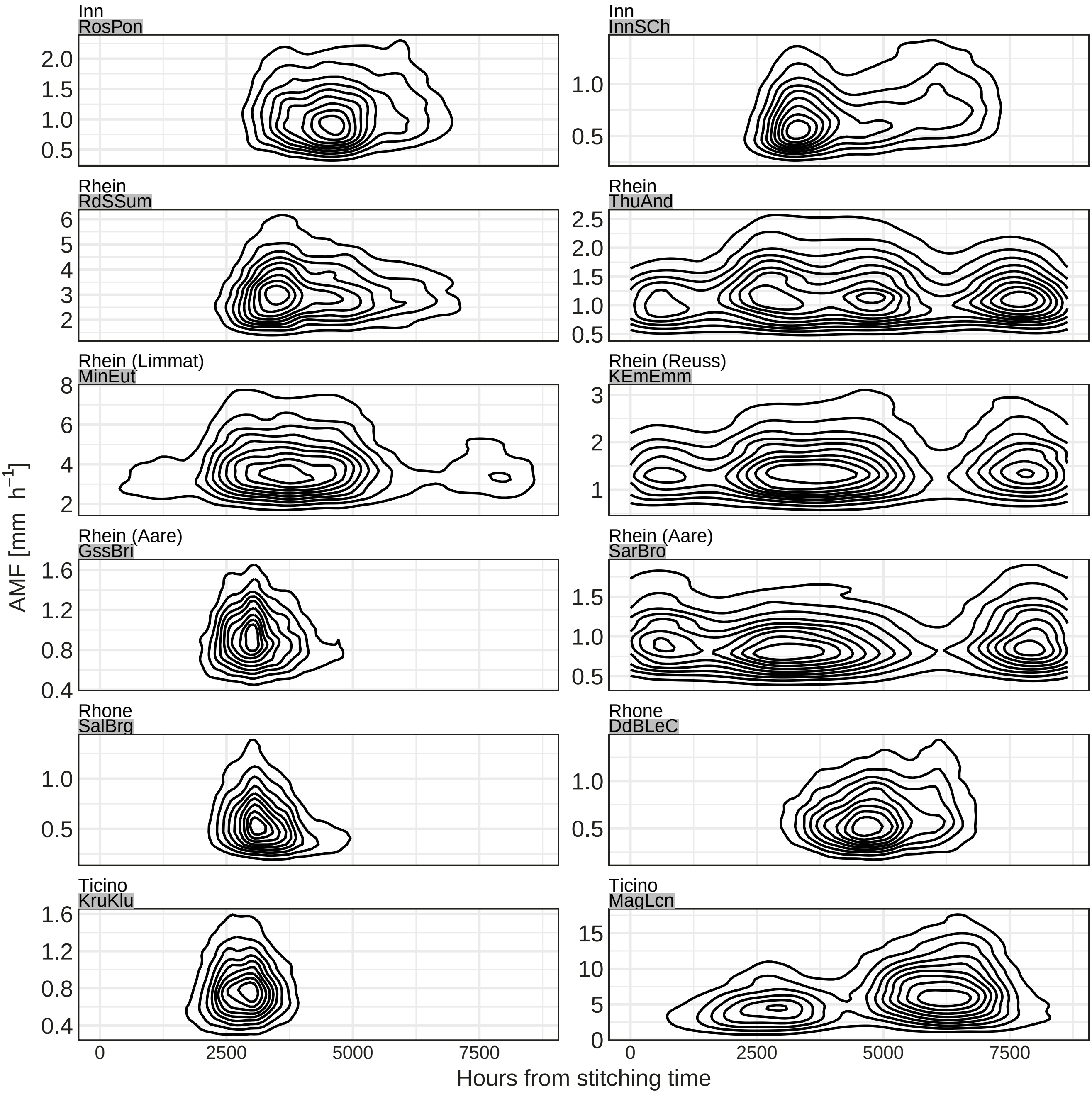

Figure S22. Contour density plots showing the magnitude of simulated AMFs as a function of their occurrence time relative to the stitching points of individual RFs. Where available, a smaller and a larger catchment was chosen for each river basin.

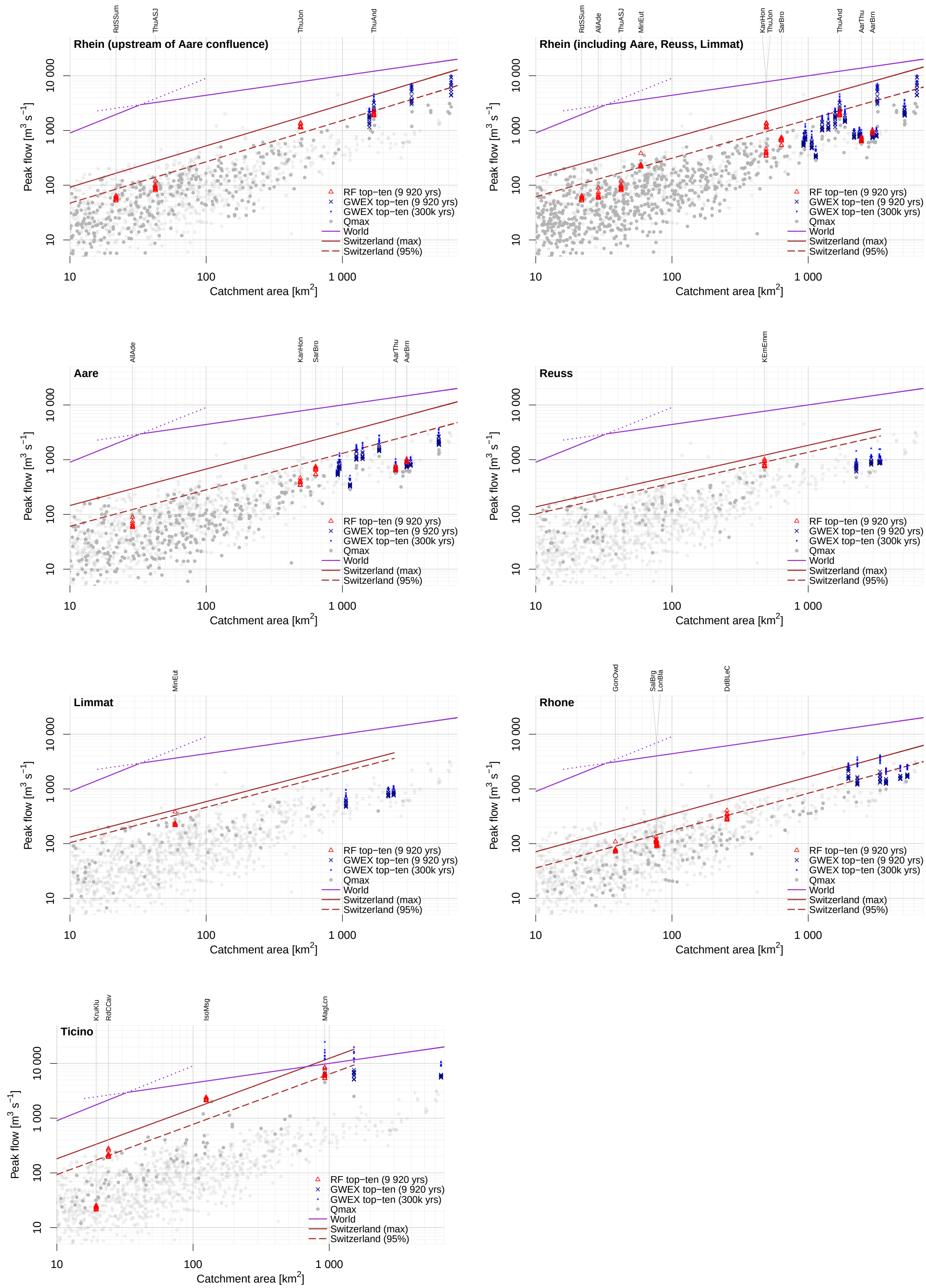

Figure S23. Highest ten annual maximum floods simulated using reforecast (RF) and weather generator (GWEX) input, presented separately for large river basins. Maximum observed floods in the corresponding large river basin (dark grey) and Switzerland (light grey) as per Kienzler and Scherrer (2018) (gray dots) are shown for context, along with an envelope curve for the corresponding large river basin (solid line: all data; dashed line: 95$^{\text{th}}$ percentile). Also shown is the envelope curve for maximum floods worldwide (Herschy, 2003). For catchment IDs see Table 1.

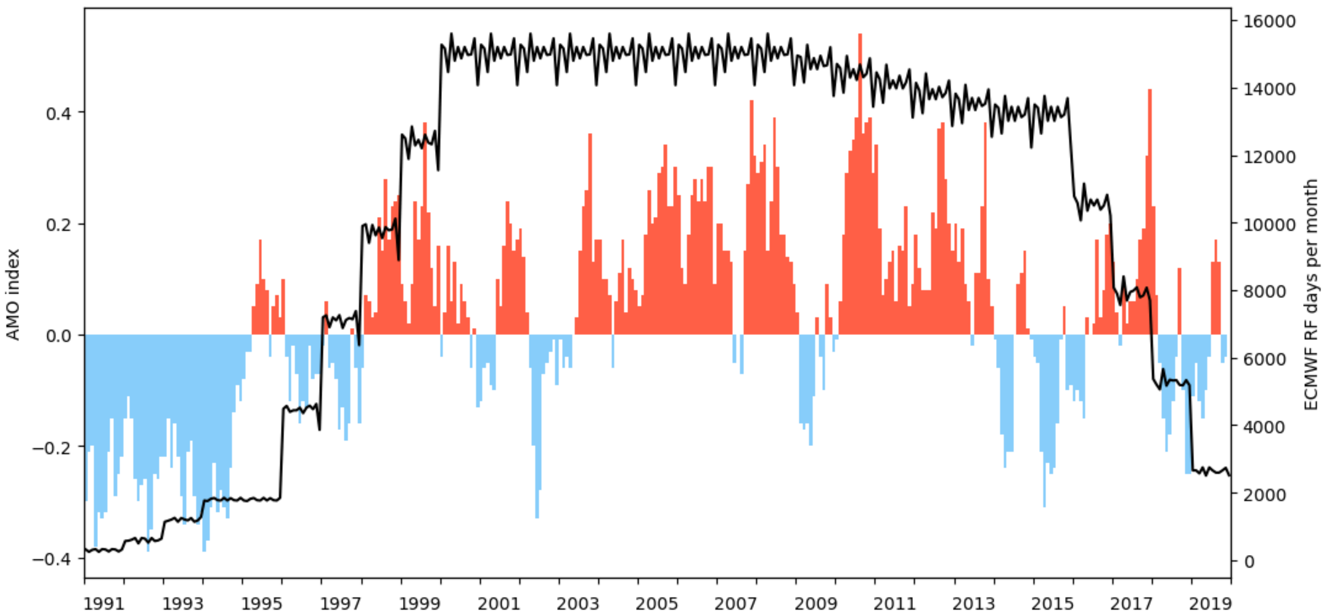

Figure S24. The Atlantic Multidecadal Oscillation (AMO) index in comparison to the sampled reofrecasts as total days within the 9920 RF years processed. The AMO data stems from NCAR and is based on Trenberth and Shea (2006) and HadISST1 (NCAR, 2023).

References

Herschy, R. W.: World Catalogue of Maximum Observed Floods, vol. 284 of *IAHS publication*, IAHS Press, Wallingford, ISBN 1-901502-47-3, 2003.

Kienzler, P. M. and Scherrer, S.: Verzeichnis grosser Hochwasserabflüsse in Schweizerischen Einzugsgebieten: Auswertung und graphische Aufbereitung, Reinach, https://www.bafu.admin.ch/bafu/de/home/themen/wasser/zustand/wasser--methoden/grosse_hochwasserabflusse-2.html, 2018.

NCAR: AMO Index Data provided by the Climate Analysis Section, NCAR, Boulder, USA, https://climatedataguide.ucar.edu/sites/default/files/2022-03/amo_monthly.txt, 2023.

Ponce, V. M.: Engineering Hydrology: Principles and Practices, Prentice Hall, ISBN 978-0133154665, 1989.

Trenberth, K. E. and Shea, D. J.: Atlantic hurricanes and natural variability in 2005, Geophysical Research Letters, 33, https://doi.org/10.1029/2006GL026894, 2006.